Acta Crystallographica Section F
**Structural Biology and Crystallization Communications**
ISSN 1744-3091

# Structure of *Escherichia coli* AdhP (ethanol-inducible dehydrogenase) with bound NAD

**Leonard M. Thomas, Angelica R. Harper, Whitney A. Miner, Helen O. Ajufo, Katie M. Branscum, Lydia Kao and Paul A. Sims***

Department of Chemistry and Biochemistry, University of Oklahoma, 101 Stephenson Parkway, Norman, OK 73019-5251, USA

Correspondence e-mail: psims@ou.edu

Received 17 May 2013
Accepted 1 June 2013

**PDB Reference:** AdhP–NAD complex, 4gkv

The crystal structure of AdhP, a recombinantly expressed alcohol dehydrogenase from *Escherichia coli* K-12 (substrain MG1655), was determined to 2.01 Å resolution. The structure, which was solved using molecular replacement, also included the structural and catalytic zinc ions and the cofactor nicotinamide adenine dinucleotide (NAD). The crystals belonged to space group $P2_1$, with unit-cell parameters $a$ = 68.18, $b$ = 118.92, $c$ = 97.87 Å, $\beta$ = 106.41°. The final $R$ factor and $R_{free}$ were 0.138 and 0.184, respectively. The structure of the active site of AdhP suggested a number of residues that may participate in a proton relay, and the overall structure of AdhP, including the coordination to structural and active-site zinc ions, is similar to those of other tetrameric alcohol dehydrogenase enzymes.

## 1. Introduction

Alcohol dehydrogenase (ADH) has held a special place in the minds of mechanistic enzymologists ever since the classical work of Westheimer and coworkers revealed the stereospecific transfer of hydrogen from the alcohol to the nicotinamide ring of the cofactor NAD (Fisher *et al.*, 1953). Relatively recently, a 'new' alcohol dehydrogenase was discovered in *Escherichia coli* when it was found that ∼17 m*M* ethanol induced the expression of an enzyme whose properties were different from the class III ADH that had previously been characterized in *E. coli* (Shafqat *et al.*, 1999). Amino-acid sequencing of the protein revealed that it was the product of the *adhP* gene (Shafqat *et al.*, 1999; Blattner *et al.*, 1997).

Similar to other ADHs, the *adhP* gene product (AdhP) catalyzes NAD/NADH-linked oxidation–reduction reactions of short-chain alcohols and aldehydes (or ketones). The enzyme allows *E. coli* to excrete ethanol when conditions require mixed-acid fermentation or to utilize ethanol as an energy source (Nosova *et al.*, 1997). Previous structures of AdhP have been reported (Karlsson *et al.*, 2003); however, the coordinate files for these structures were unavailable, which limited opportunities for comparison with the present structure. Nonetheless, the structure reported here and the previous structure of the NAD-bound enzyme (Karlsson *et al.*, 2003) show, not surprisingly, a number of similarities but also some distinct differences, as discussed below.

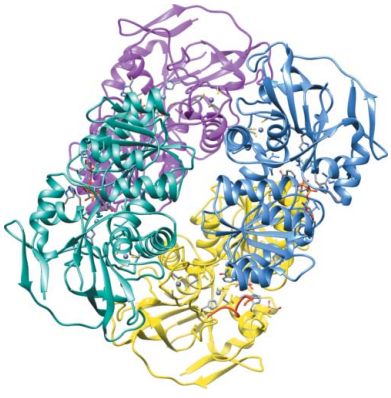

## 2. Materials and methods

### 2.1. Macromolecule production

The *adhP* gene from *E. coli* was cloned into the pET101/D-TOPO vector from Invitrogen. The resulting plasmid (pET-AdhP) was transformed into expression cells [*E. coli* BL21 (DE3)]. A 50 ml starter culture was grown for ∼9 h and was then split into two 2 l flasks that each contained 1 l LB medium plus 0.4 g $l^{-1}$ ampicillin and 16 g $l^{-1}$ lactose. Growth at 310 K and 200 rev $min^{-1}$ continued for an additional 20 h. Harvested cells were stored for around one week at 253 K and were then added to lysis buffer (0.05 *M* sodium phosphate, 0.3 *M* NaCl, 0.01 *M* imidazole pH 8) containing 0.05 g lysozyme, 0.04 g PMSF and ∼1 mg DNaseI. The mixture was shaken at 100 rev $min^{-1}$ for 2 h and then centrifuged at 15 000*g* for 15 min. The clarified supernatant was added to an Ni–NTA column and AdhP was

**Table 1**
Macromolecule-production information.

| | |
|---|---|
| Source organism | *E. coli* K-12 (substr. MG1655) |
| DNA source | Genomic DNA isolated from *E. coli* K-12 (substr. MG1655) |
| Forward primer | CACCATGAAGGCTGCAGTTGTTAC |
| Reverse primer | GTGACGGAAATCAATCACCATGC (no stop codon; read in-frame with the vector to add a V5 epitope and a $His_6$ tag) |
| Cloning vector | pET101/D-TOPO |
| Expression vector | pET101/D-TOPO (subsequently designated pET-AdhP) |
| Expression host | *E. coli* BL21 Star (DE3) |
| Complete amino-acid sequence of the construct produced | MKAAVVTKDHHVDVTYKTLRSLKHGEALLK-MECCGVCHTDLHVKNGDFGDKTGVILGH-EGIGVVAEVGPGVTSLKPGDRASVAWFYE-GCGH CEYCNSGNETLCRSVKNAGYSVDG-GMAEECIVVADYAVKVPDGLDSAAASSIT-CAGVTTYKAVKLSKIRPGQWIAIYGLGGL-GNLALQYAKN VFNAKVIAIDVNDEQLKL-ATEMGADLAINSHTEDAAKIVQEKTGGAH-AAVVTAVAKAAFNSAVDAVRAGGRVVAVG-LPPESMSLDIPRLVLD GIEVVGSLVGTRQD-LTEAFQFAAEGKVVPKVALRPLADINTIFT-EMEEGKIRGRMVIDFRHKGELNSKLEGKP-IPNPLLGLDSTRTGHHHHHH |

eluted with a 50 ml 0.02–0.25 *M* imidazole gradient. Macromolecule-production information is presented in Table 1.

### 2.2. Crystallization

Initial broad crystallization screens were set up using a Mosquito nanolitre liquid handler (TTP Labtech Inc.). Promising conditions were optimized manually using the hanging-drop vapor-diffusion method in 24-well plates. The protein concentration was 64 g $l^{-1}$ in a storage buffer consisting of 20 m*M* HEPES pH 7, 1 m*M* $MgCl_2$, 1 m*M* $NaN_3$. The final reservoir conditions were 0.2 *M* $Na_2SO_4$, 0.1 *M* bis-tris propane pH 8.5, 10 m*M* NAD, 20% PEG 3350. Single crystals were harvested using a nylon cryoloop and successively transferred into cryoprotectant solutions with increasing concentrations of glycerol (5, 10, 15 and 20%) but that otherwise matched the reservoir conditions. After the last transfer, the crystals were flash-cooled to 100 K using an Oxford Cryosystems 700 Series Cryostream.

### 2.3. Data collection and processing

X-ray diffraction data were collected on an R-AXIS IV$^{++}$ image-plate detector (Rigaku Americas Inc.) using Cu *Kα* radiation from a Rigaku RU-H3R rotating-anode generator. Image data were processed using *MOSFLM* (Leslie & Powell, 2007), with scaling and averaging performed using *SCALA* (Evans, 2006) in *CCP*4 (Winn *et al.*, 2011). Data-processing statistics are presented in Table 2.

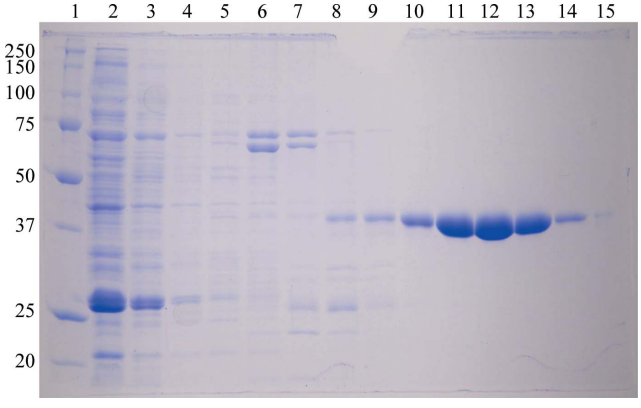


**Figure 1**
Coomassie-stained gel from the SDS–PAGE analysis of fractions eluted from the Ni–NTA column during the purification of AdhP. Lanes are as follows: 1, molecular-mass ladder (labeled in kDa); 2, load flowthrough; 3, wash flowthrough; 4–15, fractions 1–12, respectively. Fractions 7–10 were pooled, buffer exchanged/concentrated and used in crystallization trials.

**Table 2**
Data-collection and processing statistics.

Values in parentheses are for the outermost shell.

| | |
|---|---|
| Wavelength (Å) | 1.5418 |
| Temperature (K) | 100 |
| Space group | $P2_1$ |
| Unit-cell parameters (Å, °) | $a$ = 68.18, $b$ = 118.92, $c$ = 97.87, $\alpha = \gamma$ = 90.0, $\beta$ = 106.41 |
| Mosaicity (°) | 1.12 |
| Resolution range (Å) | 32.6–2.01 (2.12–2.01) |
| Total No. of reflections | 321023 |
| No. of unique reflections | 99085 |
| Completeness (%) | 99.5 (98.7) |
| Multiplicity | 3.2 (3.0) |
| $\langle I/\sigma(I)\rangle$ | 11.7 (4.7) |
| $R_{r.i.m.}$ | 0.079 (0.247) |
| Overall *B* factor from Wilson plot (Å$^2$) | 13.2 |

### 2.4. Structure solution and refinement

The crystal structure of AdhP was solved *via* molecular replacement using *Phaser* (McCoy *et al.*, 2007). The structure of *Brucella melitensis* alcohol dehydrogenase (PDB entry 3meq; Seattle Structural Genomics Center for Infectious Disease, unpublished work) was used as the initial model. The structure was refined and water molecules were added using *PHENIX* (Adams *et al.*, 2010; *phenix.refine* v.1.8_1069). Model building was performed using *Coot* (Emsley *et al.*, 2010). *MolProbity* (Chen *et al.*, 2010) was used for validiation analysis and *UCSF Chimera* (Pettersen *et al.*, 2004) was used to construct the molecular-graphics images in Figs. 2 and 3. Refinement statistics are summarized in Table 3.

## 3. Results and discussion

In the initial report that described the purification and characterization of AdhP (Shafqat *et al.*, 1999), the authors stated that wild-type AdhP bound to an Ni–NTA column; this binding was attributed to the presence of five histidine residues (only two of which were consecutive) that were located near the N-terminus of the protein. In addition to the wild-type sequence, the construct reported here contains 32 additional amino-acid residues appended to the C-terminus. These extra residues include a V5 epitope and a $His_6$ tag. As a consequence, the protein bound tightly to the Ni–NTA column and eluted relatively late in the gradient (∼0.23 *M* imidazole) in a highly pure form (Fig. 1).

A ribbon representation showing the tetrameric structure of AdhP is presented in Fig. 2. The structure of AdhP included a short peptide, which is shown in orange in the lower right-hand portion of Fig. 2. This peptide is part of the 32 extra amino-acid residues (Pro348–Leu357) that were incorporated into the construct. In all four subunits the electron density was disordered after the last naturally occurring amino acid (His336) and thus the subunit that contributed the extra density that corresponds to the above fragment is unknown.

The group that reported the previous structures of AdhP provided a number of comparisons with other ADH structures (Karlsson *et al.*, 2003). One of the previous structures of AdhP was of the apoenzyme and the other was of the holoenzyme (with bound NAD); in both cases the space group of the crystals was $P2_12_12_1$ (Karlsson *et al.*, 2003). It is expected that the previous structures and the present structure are highly similar, but the presence of the extra 32 amino-

acid residues at the C-terminus of the present structure and the observation that the crystals that led to the present structure belong to space group $P2_1$ may in part explain some of the noted differences. For example, in the previous structure of the holoenzyme three of the four subunits had bound NAD, and in these subunits the coordination to the catalytic zinc ion was of the 'classical' type in which two cysteines, a histidine and a water coordinate the zinc ion; the subunit that did not have NAD bound exhibited a different coordination of the active-site zinc ion such that the coordinating residues were the same but the water was replaced by a glutamate residue (Karlsson *et al.*, 2003). In the present structure all four subunits have bound NAD, and in each of the subunits the coordination scheme of the active-site zinc ion was of the classical type (Fig. 3).

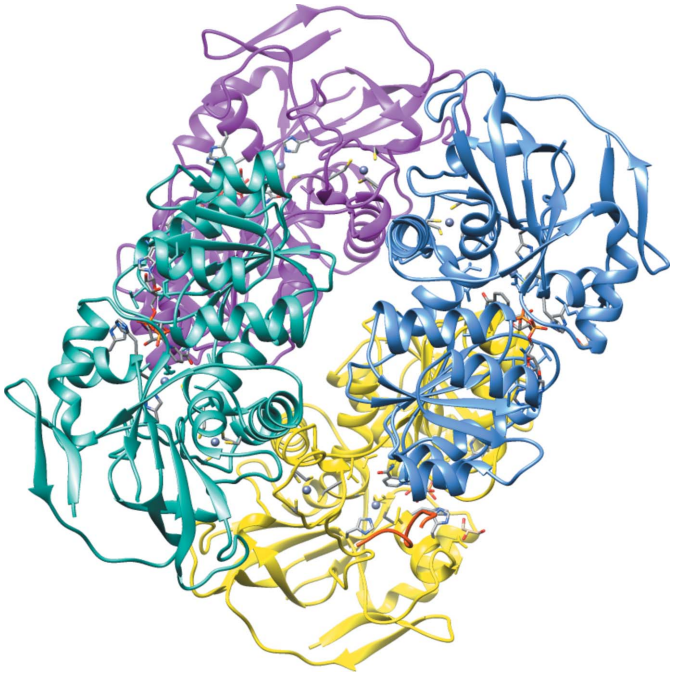

**Figure 2**
Ribbon representation of the AdhP tetramer looking down the twofold-rotation axis. Zinc ions are shown as gray spheres and NAD, glycerol, $Zn^{2+}$-coordinating residues and selected active-site residues are shown in stick form. The short peptide shown in orange at the lower right of the figure corresponds to part of the C-terminus, as discussed in the text.

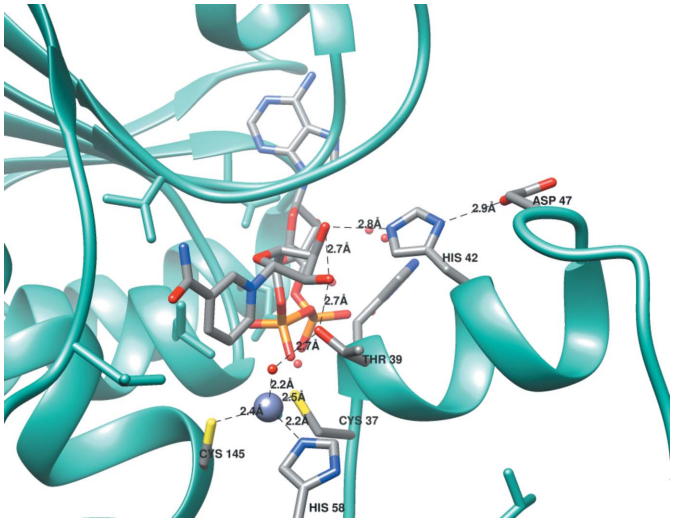


**Figure 3**
Close-up view of the active site of AdhP showing the coordinating residues of the catalytic zinc ion and the residues/moieties that may be part of a proton relay.

**Table 3**
Structure-refinement statistics.

| | |
|---|---|
| Resolution range (Å) | 32.690–2.008 |
| Completeness (%) | 99.5 |
| $\sigma$ Cutoff | 2 |
| No. of reflections, working set | 94131 |
| No. of reflections, test set | 4954 |
| Final $R_{cryst}$ | 0.138 |
| Final $R_{free}$ | 0.184 |
| No. of non-H atoms | |
| Protein | 10018 |
| Ligand | 196 |
| Solvent | 1730 |
| Total | 11944 |
| R.m.s. deviations | |
| Bonds (Å) | 0.007 |
| Angles (°) | 1.132 |
| Average *B* factors (Å$^2$) | |
| Protein | 10.3 |
| Ligand | 9.2 |
| Water | 21.0 |
| Ramachandran plot | |
| Favoured regions (%) | 97.0 |
| Additionally allowed regions (%) | 3.0 |

The structure of the AdhP active site also suggests the identities of moieties/residues that participate in a proton relay: Asp47, His42, the 2′-OH and 3′-OH of the ribose attached to the nicotinamide ring of NAD, and Thr39. A similar relay has been proposed in horse liver ADH (Luo & Bruice, 2001) and site-directed mutagenesis experiments are planned to test this hypothesis in the case of AdhP.

This work was supported in part by a Center of Biomedical Research Excellence (CoBRE) award from the National Institute of General Medical Sciences (NIGMS) of the National Institutes of Health (P20GM103640) and by funding from the University of Oklahoma. The molecular-graphics program *UCSF Chimera* was developed by the Resource for Biocomputing, Visualization and Informatics at the University of California, San Francisco with support by NIGMS P41-GM103311.

## References

Adams, P. D. *et al.* (2010). *Acta Cryst.* D**66**, 213–221.
Blattner, F. R. *et al.* (1997). *Science*, **277**, 1453–1462.
Chen, V. B., Arendall, W. B., Headd, J. J., Keedy, D. A., Immormino, R. M., Kapral, G. J., Murray, L. W., Richardson, J. S. & Richardson, D. C. (2010). *Acta Cryst.* D**66**, 12–21.
Emsley, P., Lohkamp, B., Scott, W. G. & Cowtan, K. (2010). *Acta Cryst.* D**66**, 486–501.
Evans, P. (2006). *Acta Cryst.* D**62**, 72–82.
Fisher, H. F., Conn, E. E., Vennesland, B. & Westheimer, F. H. (1953). *J. Biol. Chem.* **202**, 687–697.
Karlsson, A., El-Ahmad, M., Johansson, K., Shafqat, J., Jörnvall, H., Eklund, H. & Ramaswamy, S. (2003). *Chem. Biol. Interact.* **143–144**, 239–245.
Leslie, A. G. W. & Powell, H. R. (2007). *Evolving Methods for Macromolecular Crystallography*, edited by R. J. Read & J. L. Sussman, pp. 41–51. Dordrecht: Springer.
Luo, J. & Bruice, T. C. (2001). *J. Am. Chem. Soc.* **123**, 11952–11959.
McCoy, A. J., Grosse-Kunstleve, R. W., Adams, P. D., Winn, M. D., Storoni, L. C. & Read, R. J. (2007). *J. Appl. Cryst.* **40**, 658–674.
Nosova, T., Jousimies-Somer, H., Kaihovaara, P., Jokelainen, K., Heine, R. & Salaspuro, M. (1997). *Alcohol. Clin. Exp. Res.* **21**, 489–494.
Pettersen, E. F., Goddard, T. D., Huang, C. C., Couch, G. S., Greenblatt, D. M., Meng, E. C. & Ferrin, T. E. (2004). *J. Comput. Chem.* **25**, 1605–1612.
Shafqat, J., Höög, J. O., Hjelmqvist, L., Oppermann, U. C., Ibáñez, C. & Jörnvall, H. (1999). *Eur. J. Biochem.* **263**, 305–311.
Winn, M. D. *et al.* (2011). *Acta Cryst.* D**67**, 235–242.